Remote Sensing Letters

ISSN: 2150-704X (Print) 2150-7058 (Online) Journal homepage: http://www.tandfonline.com/loi/trsl20

Locally adaptive super-resolution waterline mapping with MODIS imagery

Wenbo Li, Xiuhua Zhang, Feng Ling & Dongbo Zheng

To cite this article: Wenbo Li, Xiuhua Zhang, Feng Ling & Dongbo Zheng (2016) Locally adaptive super-resolution waterline mapping with MODIS imagery, Remote Sensing Letters, 7:12, 1121-1130, DOI: 10.1080/2150704X.2016.1219460

To link to this article: https://doi.org/10.1080/2150704X.2016.1219460

REMOTE SENSING LETTERS, 2016
VOL. 7, NO. 12, 1121–1130
http://dx.doi.org/10.1080/2150704X.2016.1219460

Taylor & Francis
Taylor & Francis Group

Locally adaptive super-resolution waterline mapping with MODIS imagery

Wenbo Li [a], Xiuhua Zhang [b], Feng Ling [c] and Dongbo Zheng [c]

[a]Institute of Technology Innovation, Hefei Institutes of Physical Science, Chinese Academy of Sciences, Hefei Anhui, China; [b]Wuhan Institute of Technology, Wuhan, China; [c]Institute of Geodesy and Geophysics, Chinese Academy of Sciences, Wuhan, China

ABSTRACT

Mapping inland water bodies is important for relevant research fields and water resource management. Satellite remote sensing is a routine approach, and various remotely sensed images have been applied to map waterlines. MODerate-resolution Imaging Spectroradiometer (MODIS) images have advantages for waterline mapping in large areas, thanks to its wide scan width and high frequent revisiting period; however, the spatial resolution of MODIS images is too coarse to map waterlines accurately. In this article, a super-resolution mapping (SRM) model was proposed for fine spatial resolution waterline mapping with MODIS images. The proposed SRM model was directly applied in the MODIS band 2 images, which have a fine spatial resolution and a high spectral separability between water and land. In order to further take account of the spatial heterogeneity of endmembers, the reflectance values of water and land were locally calculated for each coarse resolution pixel. The proposed SRM model was assessed in two study areas located in the Tibetan Plateau, China and Wisconsin, United States, including water bodies with different areas and boundary shapes. The results showed that the accuracy values of the proposed SRM model using local endmembers were higher than those of hard classification and the SRM model using average endmembers, showing the effectiveness of the proposed model in fine spatial resolution waterline mapping with MODIS imagery.

ARTICLE HISTORY
Received 14 April 2016
Accepted 22 July 2016

1. Introduction

Inland water bodies are important parts of the Earth's water resource and play a significance role for global hydrological system. Satellite remote sensing can provide real-time information, and is a routine approach to monitor inland water bodies (Crétaux et al. 2016; Alsdorf, Rodríguez, and Lettenmaier 2007). In the last decades, a variety of remotely sensed images, such as Landsat satellite images (Frazier and Page 2000; Pardo-Pascual et al. 2012; Yang et al. 2015; Li et al. 2013b; Yamazaki, Trigg, and Ikeshima 2015), and MODerate-resolution Imaging Spectroradiometer (MODIS) images (Gao, Birkett, and Lettenmaier 2012; Chen et al. 2013; Sun, Yu, and Goldberg 2011) have been widely applied in inland water bodies monitoring.

CONTACT Feng Ling lingf@whigg.ac.cn Institute of Geodesy and Geophysics, Chinese Academy of Sciences, Wuhan 430077, China

In general, there always is a trade-off between the spatial and temporal resolutions of remotely sensed images (Priestnall and Aplin 2006). For example, the Landsat series image can map waterlines at the spatial resolution of 30 m; however, it is hard to monitor waterline changes rapidly because of its 16-day revisited time and the impact of cloud. By contrast, the MODIS image has a wide scan width and can be acquired several times every day, making it be suitable for timely water bodies monitoring in a large area. However, its coarse spatial resolution limits the accuracy of waterline mapping. Given the popular applications of MODIS imagery for global inland water bodies monitoring, improving the accuracy of waterline mapping is becoming increasingly important.

Recently, super-resolution mapping (SRM) has been a promising method to address the mixed pixel problem of remotely sensed images (Atkinson 2009; Ling et al. 2013, 2014). SRM can produce a fine spatial resolution land cover map with the input coarse spatial resolution image. SRM has been applied to improve the spatial resolution of waterlines mapped with various remotely sensed images (Huang, Chen, and Wu 2014; Li et al. 2015; Ling et al. 2008; Muslim, Foody, and Atkinson 2007; Foody, Muslim, and Atkinson 2005). Specially, several studies have been applied for MODIS images. For example, Muad and Foody (2012) fused multi-temporal sub-pixel shifted MODIS to map lakes. Li et al. (2013a) used MODIS and Shuttle Radar Topography Mission data to derivate 30-m-resolution water body maps. Wu and Liu (2015) used a statistical regression method to downscale water inundation maps. All these methods improved the accuracy of mapped waterlines; however, the results were often heavily affected by water fraction errors brought by spectral unmixing, and multiple images or additional dataset were needed in some situations, making the application is inconvenient.

The goal of this article is to propose a method to map fine spatial resolution waterlines from a single MODIS image by SRM without any other extra dataset. Different with SRM methods that use fraction images as input, the image SRM model (Ling et al. 2012; Li, Ling, and Du 2012), which can be applied on remote sensing imagery directly, was applied. Moreover, in order to overcome the shortcoming of existing image SRM models that endmember spectra are assumed to be invariant, the proposed SRM model extract locally adaptive endmember spectra for each mixed pixel, by considering the spatial relationship between water and land.

2. Study area and dataset

Two study areas were chosen in this study. Figure 1(a) shows the first area (125 km × 75 km) located in the Tibetan Plateau, China. Figure 1(b) shows the second area (36 km × 36 km) located in Wisconsin, United States. The original MODIS Level-1B file was used in order to avoid the re-projection and resampling error in standard MODIS produces. For the first study area, a cloud-free MODIS L1B swath from the Aqua satellite acquired on 25 August 2011, in which the region of interest is located close to the nadir location, was downloaded from http://reverb.echo.nasa.gov/reverb/. A Landsat Thematic Mapper (TM) image acquired on the same day was downloaded from United States Geological Survey website http://earthexplorer.usgs.gov/ and was used as the reference. For the second study area,

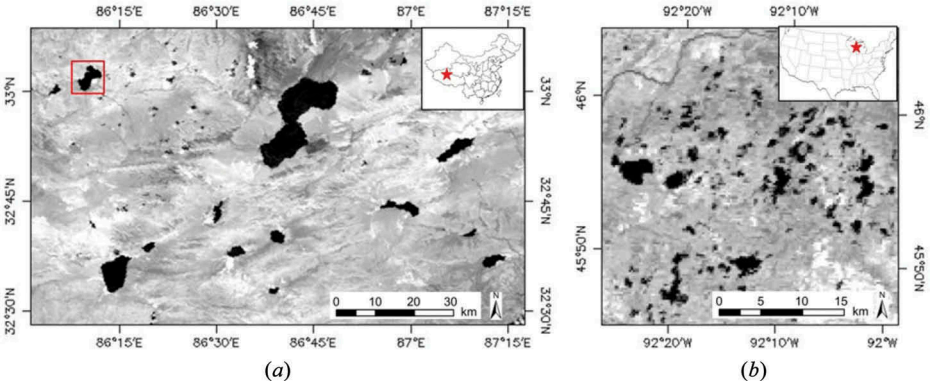

Figure 1. The MODIS band 2 images (near infrared, 841–876 nm, 250 m) in two study areas.

the used MODIS swath was acquired on 14 September 2015, and a Landsat Operational Land Imager image acquired on 15 September 2015 was used as the reference.

3. Methodology

3.1. *MODIS band selection*

In order to accurately extract fine spatial resolution waterlines from MODIS imagery by SRM, the crucial issue is reasonably using spectral and spatial information included in the image. From the spatial information, the MODIS bands 1 and 2 images have the spatial resolution of 250 m, while the MODIS bands 3–7 images have the spatial resolution of 500 m. Previous studies have shown that coarser the spatial resolution of the input image, worse the result of SRM. Then, only the first two bands are considered. For the spectral information, the band which has a high spectral separability between water and land should be used. Figure 2 shows the histograms of the MODIS bands 1 and 2 images in the first study area. The MODIS bands 2 image has a higher spectral separability between water and land than the MODIS bands 1 image, and is then more suitable for waterline mapping. Therefore, the MODIS bands 2 image is used as the input of the SRM model, because it has a fine spatial resolution and a high spectral discrimination, simultaneously.

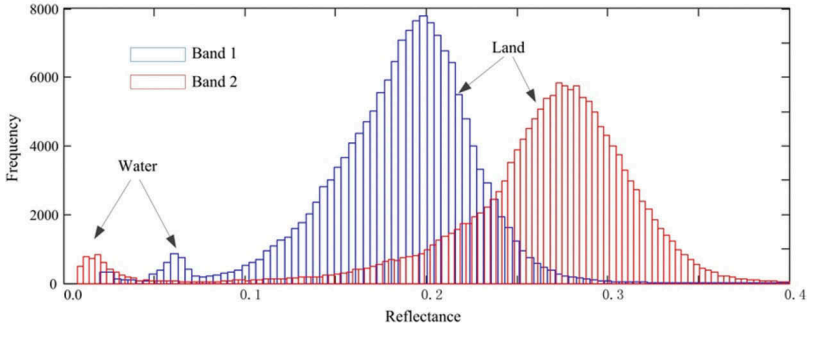

Figure 2. The histogram of reflectance of the first two 250 m bands of MODIS imagery.

3.2. *Image-based super-resolution mapping*

Let the coarse spatial resolution MODIS band 2 image be represented by an $M \times N$ array with M and N denoting the width and length of the image, respectively. We aim to map waterlines at the spatial resolution of Landsat images, that is, a spatial resolution of 30 m. Then, the zoom factor is set to be 8, and the resultant fine resolution water map has $8 \times M \times 8 \times N$ pixels. It is supposed that the reflectance value of water R_{water} and the reflectance value of land R_{land} are spatial invariant and have been known. The method applied to estimate their actual reflectance values will be discussed in detail in the next section.

Using the MODIS band 2 image as well as the water reflectance value and the land reflectance value as input, the image SRM model proposed by Ling et al. (2012) was used to produce the fine resolution waterline map x in a manner that minimizes an objective function $E(x)$, which exploits both spectral and spatial information and is expressed as:

$$\text{Min } E(x) = E^{\text{spectral}}(x) + \lambda E^{\text{spatial}}(x) \tag{1}$$

where $E^{\text{spectral}}(x)$ is the spectral term incorporating the spectral constraints provided by the input image. $E^{\text{spatial}}(x)$ is the spatial term describing the spatial pattern of waterlines in the final result. λ is the parameter used to balance the spectral term and the spatial term.

The spectral term is based on the linear mixture model and can be mathematically expressed as:

$$E^{\text{spectral}}(x) = \sum_{m=1}^{M}\sum_{n=1}^{N}\left(R_{m,n} - (R_{\text{water}} \times f_{m,n}) - (R_{\text{land}} \times (1 - f_{m,n})\right)^2 \tag{2}$$

where m and n represent coarse resolution pixel coordinates; $R_{m,n}$ is the reflectance value of the coarse resolution pixel (m,n); $f_{m,n}$ is the water areal proportion in the pixel (m,n) and $1 - f_{m,n}$ is the land areal proportion in the pixel (m,n).

The spatial term is based on the maximal spatial dependence principle and can be calculated as the sum of local spatial dependences for all fine spatial resolution pixels in the final map:

$$E^{\text{spatial}}(x) = \sum_{i=1}^{8\times M\times 8\times N}\sum_{j=1}^{W\times W}\lambda_{i,j}\varphi_{i,j} \tag{3}$$

$$\lambda_{i,j} = \frac{1}{\Omega}\exp(-d(i,j)/w) \tag{4}$$

$$\varphi_{i,j} = \begin{cases} 1 & \text{if fine resolution pixels i and j are same classes} \\ 0 & \text{otherwise} \end{cases} \tag{5}$$

where W is the size of neighbouring window, and $W \times W$ fine spatial resolution pixels are considered as neighbouring pixels of the target pixel i. $\lambda_{i,j}$ is the distance-dependent weight determined by the distance $d(i,j)$ between fine spatial resolution pixel i and its

neighbour pixel j. Ω is a normalization constant chosen in order that $\sum_{j=1}^{W\times W} \lambda_{i,j} = 1$. w is the non-linear parameter of the distance-decay model.

3.3. *Locally adaptive endmember selection*

In the image SRM model, besides the MODIS band 2 image, the reflectance values of water and land also need to be provided. In the simplest case, we can manually select representative water and land pixels from the MODIS image, and assign their averages as the reflectance values used in the model. However, it has been widely recognized that the reflectance values of different pixels belonging to the same land cover class are always much different, and the average reflectance values cannot fully explore the variability of reflectance values. For example, as shown in Figure 3(a), the difference between reflectance values of land pixels is easy to be noticed. In area A, the reflectance value is obviously higher than that in the area B. Therefore, in order to address this issue, the reflectance values of water and land are not assigned as the averages, but are locally adaptively calculated for each pixel one by one.

In order to find the local adaptive reflectance values for each coarse spatial resolution pixel in the MODIS band 2 image, pure water and land pixels are found at first. Generally, for large water bodies such as lakes and reservoirs, water and land are adjacent, and the boundary between them is the waterline. In this situation, pure water pixels are often surrounded by mixed pixels, which are in turn surrounded by pure land pixels. According to the histogram of reflectance of the MODIS band 2 image (Figure 2), water and land pixels have two respective peaks, and mixed pixels are located in the

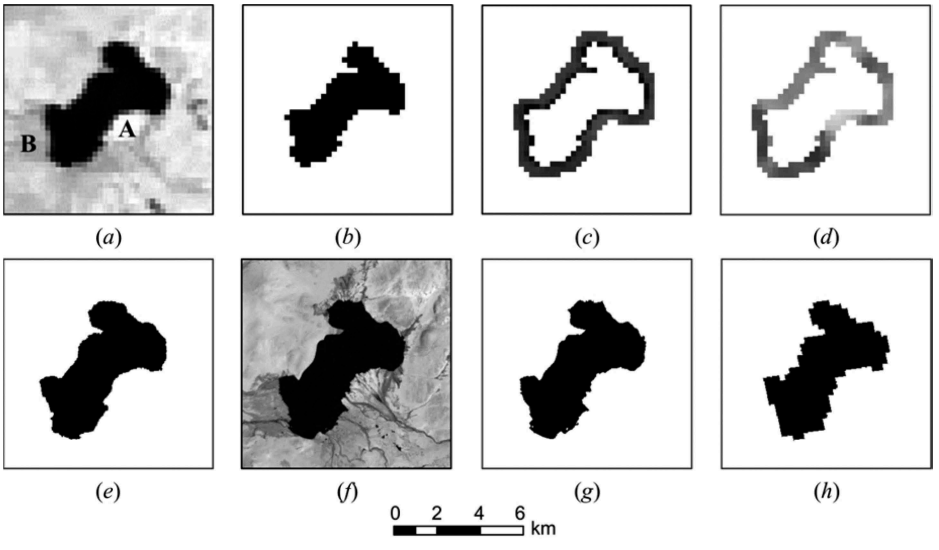

Figure 3. (a) The MODIS band 2 image of the lake indicated by the box in Figure 1(a), 'A' indicates land pixels with high reflectance values and 'B' indicates land pixels with low reflectance values; (b) extracted pure water pixels; (c) extracted mixed pixels; (d) reflectance values of land for extracted mixed pixels; (e) the SRM result; (f) the Landsat TM band 5 image; (g) the extracted reference lake from Landsat TM image; (h) the result of hard classification.

middle of the two peaks. Compared with land, the reflectance value variability of water is much less and extracting pure water pixels is expected to be more robust than extracting mixed pixels and pure land pixels directly. Therefore, in the proposed model, pure water pixels are first extracted by using a threshold that is determined with the histogram, and then mixed pixels and pure land pixels are determined according to their spatial relationship with pure water pixels.

Accurately determining pure water and land pixels from coarse spatial resolution images directly is a hard task, and they are easy to be over-estimated or under-estimated. Therefore, an iterative method is proposed to further refine the extracted pure water and land pixels. In the proposed iterative method, firstly, pure water pixels that are extracted by the threshold method are dilated using the mathematical morphology method. The expanded pixels are considered as possible mixed pixels, and rest pixels are considered as possible land pixels. Then, for each pixel, its neighbouring window with a predefined size is extracted and its water and land reflectance values are calculated from these neighbouring pixels. Specially, the reflectance values of water and land are assigned as the average values of neighbouring pure water pixels and pure land pixels, respectively. If no pure pixel can be found within the neighbouring pixel window, the reflectance value of the closest pure pixel is set to be the corresponding endmember reflectance value. Thirdly, using the estimated endmember reflectance values, the image SRM model is applied to produce an intermediate fine spatial resolution map, from which pure coarse spatial resolution water and land pixels can be determined directly. For each pixel, endmember reflectance values are re-estimated within the neighbouring window and a new intermediate fine spatial resolution map is produced. The iteration is repeated unless the estimated fine spatial resolution map does not change any more, which is considered as the final result.

The proposed method is illustrated using the lake indicated by the box in Figure 1(a) as an example. First, pure water pixels were extracted from the MODIS band 2 image shown in Figure 3(a). According to the histogram, the threshold value was set to be 0.04, and the resultant pure water pixels map are shown in Figure 3(b). Then, possible mixed pixels were extracted by dilating water pixels, with the 5×5 matrix of ones dilate template, and the result is shown in Figure 3(c). Using the extracted water pixels and land pixels, the reflectance values of endmembers were estimated for each pixel, where the size of searching neighbouring window was set to be 7×7. The reflectance values of land for all mixed pixels are shown in Figure 3(d), and it was found that these land reflectance values were much different. Using these estimated reflectance values, the fine spatial resolution water map was produced and refined iteratively. The resultant re-projected fine spatial resolution water map is shown in Figure 3(e).

3.4. *Accuracy assessment*

Landsat images were used as the reference to validate the performance of the proposed approach. Water bodies were extracted by the threshold method and used as the reference. For comparison, water bodies were also mapped from the MODIS images by using the hard classification method, and the SRM model using the average reflectance values. The user's accuracy and the producer's accuracy were calculated. The overall accuracy, which is computed using the number of correctly classified pixels to

the total number of all pixels assigned to water and actually belonging to water in the image, was also used to assess different approaches quantitatively.

4. Results

The performance of the proposed SRM model was first visually compared. Figure 3(f) shows the Landsat band 5 image and Figure 3(g) shows the extracted water map. Figure 3(h) shows the result of hard classification after re-projection. Compared with the reference high spatial resolution map, the result produced by hard classification could not represent the lake accurately. Extracted waterlines had jagged boundaries because the map produced by hard classification was based on the coarse spatial resolution. By contract, the map produced by the SRM model (Figure 3(e)) was more accurate. Extracted waterlines became smoother, and were more similar with the reference.

Figure 4 shows the results in the second study area. Similarly, maps produced by both SRM models had smooth boundaries and were superior to that produced by hard classification. Compared with the reference (Figure 4(a)), many small water bodies were not mapped by all these methods. The main reason is that no pure water pixels can be extracted in these areas. Most large water bodies, which include at least one pure water pixel, were extracted correctly. The result of the SRM model using local endmembers (Figure 4(b)) was more accurate than that of the SRM model using average endmembers (Figure 4(c)). For example, in the enlarged area shown in Figure 4, two water bodies were wrongly connected by the SRM model using average endmembers. By contrast, using local endmembers in the SRM model can overcome this problem, and two water bodies were mapped more accurate.

Quantitative statistics of maps produced by both SRM models and hard classification are shown in Table 1. In both study areas, the overall accuracy values of the SRM model using average endmembers were higher than those of hard classification. However, the user accuracy values of the SRM model using average endmembers were lower than those of hard classification. When the SRM model using local endmembers was used, values of the user accuracy, the produce accuracy and the overall accuracy were all higher than those of hard classification and the SRM model using average endmembers, showing the effectiveness of the proposed model.

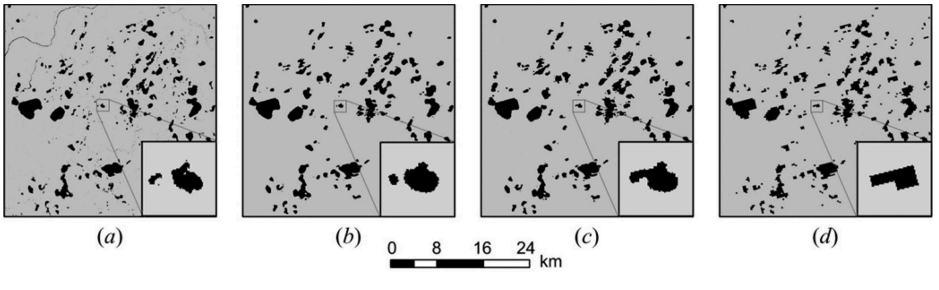

Figure 4. Water maps in the second study area produced by (a) the reference Landsat image; (b) the SRM model using local endmembers; (c) the SRM model using average endmembers and (d) hard classification.

Table 1. The user's accuracy (UA), the produce's accuracy (PA) and the overall accuracy (OA) values of different methods.

	SRM								
	Local endmembers			Average endmembers			Hard classification		
Study area	UA	PA	OA	UA	PA	OA	UA	PA	OA
A	0.977	0.985	0.963	0.947	0.957	0.909	0.958	0.934	0.898
B	0.782	0.843	0.676	0.733	0.837	0.647	0.748	0.796	0.628

5. Conclusion

This article proposed a super-resolution waterline mapping model with MODIS imagery. The MODIS band 2 image, which has a fine spatial resolution and a high spectral separability between water and land, was used as the input image. In the SRM model, the reflectance values of water and land are locally calculated for each pixel in order to take account of the spatial heterogeneity. The experiment results showed that the SRM model using local endmembers produced water bodies with a higher accuracy than those produced by the SRM model using average endmembers and hard classification. The results also indicted that when the size of water bodies was too small and no pure water pixel existed, the water bodies could not be mapped correctly.

The proposed SRM model can use a single MODIS band to map waterlines at the sub-pixel scale and does not need any other additional dataset, making the application convenient. In practice, because MODIS has a wide-swath and a high temporal resolution, it could be used for timely inland water bodies monitoring in a large area. Therefore, applying the proposed SRM model on MODIS imagery provides an alternative solution when other fine spatial resolution satellite images, such as Landsat images, are unavailable.

Disclosure statement

No potential conflict of interest was reported by the authors.

Funding

This work was supported by the National Natural Science Foundation of China [61305039], the National Key Technologies Research and Development Program of China [2016YFB0502604] and the Distinguished Young Scientist Grant of the Chinese Academy of Sciences.

ORCID

Wenbo Li http://orcid.org/0000-0002-0464-6955
Xiuhua Zhang http://orcid.org/0000-0003-3193-2292
Feng Ling http://orcid.org/0000-0002-0685-4897
Dongbo Zheng http://orcid.org/0000-0002-8932-0750

References

Alsdorf, D. E., E. Rodríguez, and D. P. Lettenmaier. 2007. "Measuring Surface Water from Space." *Reviews of Geophysics* 45: 2. doi:10.1029/2006RG000197.

Atkinson, P. M. 2009. "Issues of Uncertainty in Super-Resolution Mapping and Their Implications for the Design of an Inter-Comparison Study." *International Journal of Remote Sensing* 30 (20): 5293–5308. doi:10.1080/01431160903131034.

Chen, Y., C. Huang, C. Ticehurst, L. Merrin, and P. Thew. 2013. "An Evaluation of MODIS Daily and 8-Day Composite Products for Floodplain and Wetland Inundation Mapping." *Wetlands* 33 (5): 823–835. doi:10.1007/s13157-013-0439-4.

Crétaux, J.-F., R. Abarca-del-Río, M. Bergé-Nguyen, A. Arsen, V. Drolon, G. Clos, and P. Maisongrande. 2016. "Lake Volume Monitoring from Space." *Surveys in Geophysics* 37 (2): 269–305. doi:10.1007/s10712-016-9362-6.

Foody, G. M., A. M. Muslim, and P. M. Atkinson. 2005. "Super-Resolution Mapping of the Waterline from Remotely Sensed Data." *International Journal of Remote Sensing* 26 (24): 5381–5392. doi:10.1080/01431160500213292.

Frazier, P. S., and K. J. Page. 2000. "Water Body Detection and Delineation with Landsat TM Data." *Photogrammetric Engineering and Remote Sensing* 66 (12): 1461–1468.

Gao, H. L., C. Birkett, and D. P. Lettenmaier. 2012. "Global Monitoring of Large Reservoir Storage from Satellite Remote Sensing." *Water Resources Research* 48: 9. doi:10.1029/2012WR012063.

Huang, C., Y. Chen, and J. P. Wu. 2014. "DEM-Based Modification of Pixel-Swapping Algorithm for Enhancing Floodplain Inundation Mapping." *International Journal of Remote Sensing* 35 (1): 365–381. doi:10.1080/01431161.2013.871084.

Li, L. Y., Y. Chen, T. B. Xu, R. Liu, K. F. Shi, and C. Huang. 2015. "Super-Resolution Mapping of Wetland Inundation from Remote Sensing Imagery Based on Integration of Back-Propagation Neural Network and Genetic Algorithm." *Remote Sensing of Environment* 164: 142–154. doi:10.1016/j.rse.2015.04.009.

Li, S. M., D. L. Sun, M. Goldberg, and A. Stefanidis. 2013a. "Derivation of 30-M-Resolution Water Maps from TERRA/MODIS and SRTM." *Remote Sensing of Environment* 134: 417–430. doi:10.1016/j.rse.2013.03.015.

Li, W., Z. Du, F. Ling, D. Zhou, H. Wang, Y. Gui, B. Sun, and X. Zhang. 2013b. "A Comparison of Land Surface Water Mapping Using the Normalized Difference Water Index from TM, ETM+ and ALI." *Remote Sensing* 5 (11): 5530–5549. doi:10.3390/rs5115530.

Li, X., F. Ling, and Y. Du. 2012. "Super-Resolution Mapping Based on the Supervised Fuzzy C-Means Approach." *Remote Sensing Letters* 3 (6): 501–510. doi:10.1080/01431161.2011.631607.

Ling, F., Y. Du, X. Li, W. Li, F. Xiao, and Y. Zhang. 2013. "Interpolation-Based Super-Resolution Land Cover Mapping." *Remote Sensing Letters* 4 (7): 629–638. doi:10.1080/2150704X.2013.781284.

Ling, F., Y. Du, F. Xiao, and X. Li. 2012. "Subpixel Land Cover Mapping by Integrating Spectral and Spatial Information of Remotely Sensed Imagery." *IEEE Geoscience and Remote Sensing Letters* 9 (3): 408–412. doi:10.1109/LGRS.2011.2169934.

Ling, F., X. Li, F. Xiao, and Y. Du. 2014. "Superresolution Land Cover Mapping Using Spatial Regularization." *IEEE Transactions on Geoscience and Remote Sensing* 52 (7): 4424–4439. doi:10.1109/tgrs.2013.2281992.

Ling, F., F. Xiao, Y. Du, H. P. Xue, and X. Y. Ren. 2008. "Waterline Mapping at the Subpixel Scale from Remote Sensing Imagery with High-Resolution Digital Elevation Models." *International Journal of Remote Sensing* 29 (6): 1809–1815. doi:10.1080/01431160701802489.

Muad, A. M., and G. M. Foody. 2012. "Super-Resolution Mapping of Lakes from Imagery with a Coarse Spatial and Fine Temporal Resolution." *International Journal of Applied Earth Observation and Geoinformation* 15: 79–91. doi:10.1016/j.jag.2011.06.002.

Muslim, M. A., G. M. Foody, and P. M. Atkinson. 2007. "Shoreline Mapping from Coarse-Spatial Resolution Remote Sensing Imagery of Seberang Takir, Malaysia." *Journal of Coastal Research* 236: 1399–1408. doi:10.2112/04-0421.1.

Pardo-Pascual, J. E., C. J. Almonacid, L. A. Ruiz, and J. Palomar-Vázquez. 2012. "Automatic Extraction of Shorelines from Landsat TM and ETM+ Multi-Temporal Images with Subpixel Precision." *Remote Sensing of Environment* 123: 1–11. doi:10.1016/j.rse.2012.02.024.

Priestnall, G., and P. Aplin. 2006. "Cover: Spatial and Temporal Remote Sensing Requirements for River Monitoring." *International Journal of Remote Sensing* 27 (11): 2111–2120. doi:10.1080/01431160500396139.

Sun, D. L., Y. Y. Yu, and M. D. Goldberg. 2011. "Deriving Water Fraction and Flood Maps from MODIS Images Using a Decision Tree Approach." *IEEE Journal of Selected Topics in Applied Earth Observations and Remote Sensing* 4 (4): 814–825. doi:10.1109/JSTARS.2011.2125778.

Wu, G. P., and Y. B. Liu. 2015. "Downscaling Surface Water Inundation from Coarse Data to Fine-Scale Resolution: Methodology and Accuracy Assessment." *Remote Sensing* 7 (12): 15989–16003. doi:10.3390/rs71215813.

Yamazaki, D., M. A. Trigg, and D. Ikeshima. 2015. "Development of a Global ~90 M Water Body Map Using Multi-Temporal Landsat Images." *Remote Sensing of Environment* 171: 337–351. doi:10.1016/j.rse.2015.10.014.

Yang, Y. H., Y. X. Liu, M. X. Zhou, S. Y. Zhang, W. F. Zhan, C. Sun, and Y. W. Duan. 2015. "Landsat 8 OLI Image Based Terrestrial Water Extraction from Heterogeneous Backgrounds Using a Reflectance Homogenization Approach." *Remote Sensing of Environment* 171: 14–32. doi:10.1016/j.rse.2015.10.005.